2. **Baker, T., and H. Cheng.** 1996. A model based approach for determining orientations of biological macromolecules imaged by cryo-electron microscopy. J. Struct. Biol. **116:**120–130.

3. **Bendall, R. P., V. Ellis, S. Ijaz, P. Thurairajah, and H. R. Dalton.** 2008. Serological response to hepatitis E virus genotype 3 infection: IgG quantitation, avidity, and IgM response. J. Med. Virol. **80:**95–101.

4. **Crowther, R. A.** 1971. Procedures for three-dimensional reconstruction of spherical viruses by Fourier synthesis from electron micrographs. Philos. Trans. R. Soc. Lond. B Biol. Sci. **261:**221–230.

5. **DeLano, W. L.** 2002. The PYMOL molecular graphics system. DeLano Scientific, Palo Alto, CA.

6. **Deshmukh, T. M., K. S. Lole, A. S. Tripathy, and V. A. Arankalle.** 2007. Immunogenicity of candidate hepatitis E virus DNA vaccine expressing complete and truncated ORF2 in mice. Vaccine **25:**4350–4360.

7. **Emerson, S., P. Clemente-Casares, N. Moiduddin, V. A. Arankalle, U. Torian, and R. Purcell.** 2006. Putative neutralization epitopes and broad cross-genotype neutralization of hepatitis E virus confirmed by a quantitative cell-culture assay. J. Gen. Virol. **87:**697–704.

8. **Guu, T., Z. Liu, Q. Ye, D. Mata, K. Li, C. Yin, J. Zhang, and Y. Tao.** 2009. Structure of the hepatitis E virus-like particle suggests mechanisms for virus assembly and receptor binding. Proc. Natl. Acad. Sci. U. S. A. **106:**12992–12997.

9. **Jones, T. A., J. Y. Zou, S. W. Cowan, and M. Kjeldgaard.** 1991. Improved method for building protein models in electron density maps and the location of errors in these models. Acta Crystallogr. A **47**(Pt. 2):110–119.

10. **Khuroo, M. S., and M. S. Khuroo.** 2008. Hepatitis E virus. Curr. Opin. Infect. Dis. **21:**539–543.

11. **Li, S., S. Tang, J. Seetharaman, C. Y. Yang, Y. Gu, J. Zhang, H. Du, J. W. Shih, C. L. Hew, J. Sivaraman, and N. S. Xia.** 2009. Dimerization of hepatitis E virus capsid protein E2s domain is essential for virus-host interaction. PLoS Pathog. **5:**e1000537.

12. **Li, T.-C., Y. Suzaki, Y. Ami, T. N. Dhole, T. Miyamura, and N. Takeda.** 2004. Protection of cynomolgus monkeys against HEV infection by oral administration of recombinant hepatitis E virus-like particles. Vaccine **22:**370–377.

13. **Li, T.-C., N. Takeda, T. Miyamura, Y. Matsuura, J. C. Y. Wang, H. Engvall, L. Hammar, L. Xing, and R. H. Cheng.** 2005. Essential elements of the capsid protein for self-assembly into empty virus-like particles of hepatitis E virus. J. Virol. **79:**12999–13006.

14. **Li, T., N. Takeda, and T. Miyamura.** 2001. Oral administration of hepatitis E virus-like particles induces a systemic and mucosal immune response in mice. Vaccine **19:**3476–3484.

15. **Li, T. C., Y. Yamakawa, K. Suzuki, M. Tatsumi, M. A. Razak, T. Uchida, N. Takeda, and T. Miyamura.** 1997. Expression and self-assembly of empty virus-like particles of hepatitis E virus. J. Virol. **71:**7207–7213.

16. **Maloney, B. J., N. Takeda, Y. Suzaki, Y. Ami, T. C. Li, T. Miyamura, C. J. Arntzen, and H. S. Mason.** 2005. Challenges in creating a vaccine to prevent hepatitis E. Vaccine **23:**1870–1874.

17. **Minuk, G. Y., A. Sun, D. F. Sun, J. Uhanova, L. E. Nicolle, B. Larke, and A. Giulivi.** 2007. Serological evidence of hepatitis E virus infection in an indigenous North American population. Can J. Gastroenterol. **21:**439–442.

18. **Mushahwar, I. K.** 2008. Hepatitis E virus: molecular virology, clinical features, diagnosis, transmission, epidemiology, and prevention. J. Med. Virol. **80:**646–658.

19. **Naik, S. R., R. Aggarwal, P. N. Salunke, and N. N. Mehrotra.** 1992. A large waterborne viral hepatitis E epidemic in Kanpur, India. Bull. World Health Organ. **70:**597–604.

20. **Niikura, M., S. Takamura, G. Kim, S. Kawai, M. Saijo, S. Morikawa, I. Kurane, T. C. Li, N. Takeda, and Y. Yasutomi.** 2002. Chimeric recombinant hepatitis E virus-like particles as an oral vaccine vehicle presenting foreign epitopes. Virology **293:**273–280.

21. **Pavio, N., and J. M. Mansuy.** 2010. Hepatitis E in high-income countries. Curr. Opin. Infect. Dis. **23:**521–527.

22. **Pettersen, E. F., T. D. Goddard, C. C. Huang, G. S. Couch, D. M. Greenblatt, E. C. Meng, and T. E. Ferrin.** 2004. UCSF Chimera—a visualization system for exploratory research and analysis. J. Comput. Chem. **25:**1605–1612.

23. **Riddell, M. A., F. Li, and D. A. Anderson.** 2000. Identification of immunodominant and conformational epitopes in the capsid protein of hepatitis E virus by using monoclonal antibodies. J. Virol. **74:**8011–8017.

24. **Robinson, R. A., W. H. Burgess, S. U. Emerson, R. S. Leibowitz, S. A. Sosnovtseva, S. Tsarev, and R. H. Purcell.** 1998. Structural characterization of recombinant hepatitis E virus ORF2 proteins in baculovirus-infected insect cells. Protein Expr. Purif. **12:**75–84.

25. **Schofield, D. J., J. Glamann, S. U. Emerson, and R. H. Purcell.** 2000. Identification by phage display and characterization of two neutralizing chimpanzee monoclonal antibodies to the hepatitis E virus capsid protein. J. Virol. **74:**5548–5555.

26. **Schofield, D. J., R. H. Purcell, H. T. Nguyen, and S. U. Emerson.** 2003. Monoclonal antibodies that neutralize HEV recognize an antigenic site at the carboxyterminus of an ORF2 protein vaccine. Vaccine **22:**257–267.

27. **Tsarev, S. A., T. S. Tsareva, S. U. Emerson, S. Govindarajan, M. Shapiro, J. L. Gerin, and R. H. Purcell.** 1997. Recombinant vaccine against hepatitis E: dose response and protection against heterologous challenge. Vaccine **15:**1834–1838.

28. **Worm, H. C., and G. Wirnsberger.** 2004. Hepatitis E vaccines: progress and prospects. Drugs **64:**1517–1531.

29. **Xiao, C., and M. G. Rossmann.** 2007. Interpretation of electron density with stereographic roadmap projections. J. Struct. Biol. **158:**181–186.

30. **Xing, L., K. Kato, T. Li, N. Takeda, T. Miyamura, L. Hammar, and R. H. Cheng.** 1999. Recombinant hepatitis E capsid protein self-assembles into a dual-domain T=1 particle presenting native virus epitopes. Virology **265:**35–45.

31. **Xing, L., T. C. Li, N. Miyazaki, M. N. Simon, J. S. Wall, M. Moore, C. Y. Wang, N. Takeda, T. Wakita, T. Miyamura, and R. H. Cheng.** 2010. Structure of hepatitis E virion-sized particle reveals an RNA-dependent viral assembly pathway. J. Biol. Chem. **285:**33175–33183.

32. **Yamashita, T., Y. Mori, N. Miyazaki, H. Cheng, M. Yoshimura, H. Unno, R. Shima, K. Moriishi, T. Tsukihara, T. C. Li, N. Takeda, T. Miyamura, and Y. Matsuura.** 2009. Biological and immunological characteristics of hepatitis E virus-like particles based on the crystal structure. Proc. Natl. Acad. Sci. U. S. A. **106:**12986–12991.

33. **Zhou, Y. H., R. Purcell, and S. Emerson.** 2005. A truncated ORF2 protein contains the most immunogenic site on ORF2: antibody responses to nonvaccine sequences following challenge of vaccinated and nonvaccinated macaques with hepatitis E virus. Vaccine **23:**3157–3165.

Acquisition of HIV-1 Resistance in T Lymphocytes Using an ACA-Specific *E. coli* mRNA Interferase

Hideto Chono,[1,2] Kazuya Matsumoto,[1] Hiroshi Tsuda,[1,2] Naoki Saito,[1,2] Karim Lee,[3]
Sujeong Kim,[4] Hiroaki Shibata,[5] Naohide Ageyama,[5] Keiji Terao,[5] Yasuhiro Yasutomi,[5]
Junichi Mineno,[1] Sunyoung Kim,[3] Masayori Inouye,[6] and Ikunoshin Kato[1,2]

Abstract

Transcriptional activation of gene expression directed by the long terminal repeat (LTR) of HIV-1 requires both the transactivation response element (TAR) and Tat protein. HIV-1 mutants lacking a functional *tat* gene are not able to proliferate. Here we take a genetic approach to suppress HIV-1 replication based on Tat-dependent production of MazF, an ACA-specific endoribonuclease (mRNA interferase) from *Escherichia coli*. When induced, MazF is known to cause Bak- and NBK-dependent apoptotic cell death in mammalian cells. We first constructed a retroviral vector, in which the *mazF* (ACA-less) gene was inserted under the control of the HIV-1 LTR, which was then transduced into CD4+ T-lymphoid CEM-SS cells in such a way that, upon HIV-1 infection, the *mazF* gene is induced to destroy the infecting HIV-1 mRNA, preventing HIV-1 replication. Indeed, when the transduced cells were infected with HIV-1 IIIB, the viral replication was effectively inhibited, as HIV-1 IIIB p24 could not be detected in the culture medium. Consistently, not only cell growth but also the CD4 level was not affected by the infection. These results suggest that the HIV-1-LTR-regulated *mazF* gene was effectively induced upon HIV-1 IIIB infection, which is sufficient enough to destroy the viral mRNA from the infected HIV-1 IIIB to completely block viral proliferation in the cells, but not to affect normal cell growth. These results indicate that the T cells transduced with the HIV-1-LTR-regulated *mazF* gene acquire HIV-1 resistance, providing an intriguing potential for the use of the HIV-1-LTR-regulated *mazF* gene in anti-HIV gene therapy.

Introduction

R NASE-BASED STRATEGIES for anti-human immunodeficiency virus (HIV) gene therapy may be superior to RNA-based (antisense, ribozyme, or siRNAs) strategies, because the former strategies evade the effects of frequent resistant mutations in HIV-1. MazF is a unique sequence-specific endoribonuclease, or mRNA interferase, encoded by the *Escherichia coli* genome (Zhang *et al.*, 2003). It cleaves mRNA at ACA-specific sequences and effectively inhibits protein synthesis. To date, a number of MazF homologues have been found in various bacteria. These homologues have a wide range of sequence specificities and cleave three- to five-nucleotide RNA sequences in transcripts that play diverse roles in bacterial physiology (Zhu *et al.*, 2006, Yamaguchi and Inouye, 2009), including cell-growth regulation, specific gene

regulation (Zhu *et al.*, 2009), and obligatory programmed cell death (Nariya and Inouye, 2008). Induction of *E. coli* MazF mRNA interferase in mammalian cells has been demonstrated to effectively induce Bak- and NBK-dependent apoptotic cell death (Shimazu *et al.*, 2007), indicating that MazF mRNA interferase may be a new and effective tool for gene therapy.

In the HIV-1 life cycle immediately after HIV-1 infection, Tat (transactivator of transcription), an early regulatory protein encoded by the HIV-1 genome, is produced, which subsequently binds to the TAR (transactivation response) sequence to induce the transcription of the HIV-1 genome leading to the expression of other HIV-1 proteins (Berkhout *et al.*, 1989). Therefore, for prevention of HIV-1 infection, it would be a best strategy to preferentially destroy the HIV-1 transcript upon HIV-1 infection. For this purpose, we constructed a Tat-dependent MazF expression system in a

[1]Center for Cell and Gene Therapy, Takara Bio Inc., Otsu, Shiga, 520-2193, Japan.
[2]Biotechnology Research Laboratories, Takara Bio Inc., Otsu, Shiga, 520-2193, Japan.
[3]Department of Biological Sciences, Seoul National University, Seoul 151-742, Korea.
[4]ViroMed Co. Ltd., Seoul 151-818, Korea.
[5]Tsukuba Primate Research Center, National Institute of Biomedical Innovation, Tsukuba, Ibaraki, 305-0843, Japan.
[6]Department of Biochemistry, Robert Wood Johnson Medical School, Piscataway, NJ 08854, USA.

35

retroviral vector, in which the *mazF* gene was fused downstream of the TAR sequence. As the *E. coli mazF* open-reading frame contains nine ACA sequences, all of them were engineered to MazF-uncleavable sequences without changing the amino acid sequence of MazF. This vector was then transduced into T cells so that MazF production is expected to be induced upon HIV-1 infection. Note that Tat protein produced upon HIV-1 infection induces not only the transcription of infected HIV-1, but also the transcription of the HIV-1 long terminal repeat (LTR)-regulated *mazF* (ACA-less) gene integrated into the genome of the T cells. In the present article, CD4+ T lymphoid line CEM-SS cells were used as T cells, which were transduced with the retroviral vector containing the Tat-inducible *mazF* (ACA-less) gene under the HIV-1-LTR promoter. When the transduced cells were infected with HIV-1 IIIB, the replication of the infected virus was effectively inhibited without affecting cell growth. Notably, the CD4 level after HIV-1 IIIB infection was not affected either. These results suggest that the HIV-1-LTR-regulated *mazF* (ACA-less) gene was effectively induced upon HIV-1 IIIB infection, which is sufficient enough to destroy the viral mRNA from the infected HIV-1 IIIB to completely block viral proliferation in the cells. However, the level of MazF induced is not enough to cause any serious cellular damage, thus maintaining normal cell growth and the CD4 level. These results suggest an intriguing potential for the use of the HIV-1-LTR-regulated *mazF* (ACA-less) gene in anti-HIV gene therapy.

Materials and Methods

Cell lines

293T (ATCC no. CRL-11268) cells were cultured in Dulbecco's modified Eagle medium (DMEM; Sigma-Aldrich, Steinheim, Germany) supplemented with 10% (v/v) fetal bovine serum (FBS; Invitrogen, Carlsbad, CA). CEM-SS cells (Kim *et al.*, 1989) were cultured in RPMI-1640 (Sigma-Aldrich) containing 10% (v/v) FBS (Invitrogen). The doubling time of the cells for each culture condition was calculated by linear regression analysis using Microsoft Excel software (Microsoft, Seattle, WA).

Retroviral vectors

The self-inactivating retroviral vector pMTD3 was constructed by deleting a segment consisting of 267 nucleotides from the 3′LTR U3 region of pMT (Lee *et al.*, 2004). An ACA-less *mazF* gene was synthesized by engineering all nine ACA sequences in the original *E. coli mazF* gene to MazF-uncleavable sequences without changing the amino acid sequence of MazF. The HIV-LTR fragment was obtained from pQBI-LTRgagGFP (Quantum Biotechnologies Inc., Montreal, QC, Canada). To minimize the HIV-LTR sequence, U3-TAR fragments were obtained by PCR. The ACA-less *mazF* gene was inserted downstream of U3-TAR to obtain the final self-inactivating retroviral vector plasmid, pMTD3-U3TAR-MazF. As a control, the green fluorescent protein (GFP) gene was inserted into the vector to obtain pMTD3-U3TAR-GFP.

To mimic HIV replication, two kinds of retroviral vectors that express the HIV-1 Tat protein were constructed as follows: (1) Constitutitve Tat expression system from MLV-LTR. The HIV-1 *tat* gene was synthesized and inserted

at the multiple-cloning site of pMT. To easily monitor the gene expression in transduced cells, an internal ribosome entry site (IRES) and a coding region for a fluorescent protein, ZsGreen, were fused downstream of the *tat* gene. Thus, the resulting plasmid, pM-LTR-Tat-ZG, expresses Tat as well as ZsGreen from MLV-LTR. (2) Tat expression system from the HIV-1 LTR. The HIV-LTR-*tat*-polyA cassette was inserted in the opposite direction of pMT, and the ZsGreen marker gene was expressed from a phosphoglycerate kinase (PGK) promoter in the normal orientation of pMT. The resulting vector plasmid was designated as pH-LTR-Tat-ZG.

To enhance the viral titer for efficient *mazF* gene transduction, the HIV-LTR-MazF-polyA cassette was introduced in the opposite direction of the MoMLV-LTR at the multicloning site of pMT plasmid (Lee *et al.*, 2004). A truncated form of the human low-affinity nerve growth factor gene (ΔLNGFR) (Verzeletti *et al.*, 1998) was also introduced into the retrovirus vector as a surface marker. The ΔLNGFR gene is under the control of human PGK promoter. The resultant vector plasmid was designated as pMT-MFR-PL2 (Fig. 1B).

Preparation of retroviral vectors

The self-inactivating retroviral vector was generated by the transient transfection method as follows: The GALV-*env* expression vector plasmid, pVM-GeR, was constructed by replacing the amphotropic-*env* gene of pVM-AE (Yu *et al.*, 2003) with the gibbon ape leukemia virus envelope gene. The GALV-env retroviral vector was produced by co-transfecting 293T cells with the retroviral *gag-pol* expression vector plasmid, pVM-GP (Yu *et al.*, 2003), pVM-GeR, and the self-inactivating retroviral vector plasmid. Two days after transfection, viral supernatant was harvested by filtration of the culture fluid from 293T cells with use of a 0.45-μm filter.

GALV-enveloped retroviral Tat expression vectors and MazF expression vector were also generated as follows: Ecotropic retroviral vectors were generated by the transient transfection method using the packaging plasmids pGP (MLV-*gag-pol*; Takara Bio, Otsu, Shiga, Japan) and pE-eco (ecotropic *env*; Takara Bio) with the retroviral vector plasmid pM-LTR-Tat-ZG, pH-LTR-Tat-ZG, or pMT-MFR-PL2. This was performed with use of human embryonic kidney 293T-derived G3T-hi cells (Takara Bio) by using the calcium phosphate co-transfection method. The GALV-*env* retroviral vector was obtained from PG13 packaging cells (ATCC no. CRL-10686) by infection with the ecotropic retrovirus vector as prepared above. After selection of the infected PG13 cells, the virus was collected from the growth medium by filtration of the supernatant with use of a low-protein binding filter (0.45 μm).

Retroviral transduction into CEM-SS cells

CEM-SS cells were infected with self-inactivating retroviral vectors in the presence of 8 μg/ml Polybrene (hexadimethrine bromide; Sigma-Aldrich). Polyclonal gene-transduced cell populations were obtained by selecting the cells with G418 (Invitrogen) at a concentration of 1 mg/ml.

CEM-SS cells or CEM-SS cells transduced with MTD3-U3TAR-MazF were infected with Tat expression retroviral vectors M-LTR-Tat-ZG or H-LTR-Tat-ZG in the presence of RetroNectin (Takara Bio) according to the manufacturer's protocol.

FIG. 1. Construction of retroviral vector under the control of HIV-LTR promoter. To remove promoter activity of the MoMLV LTR, the self-inactivating retroviral vector pMTD3 was constructed based on pMT (Lee *et al.,* 2004) by deleting a 276-bp fragment from its 3'LTR U3 region. A synthetic ACA-less *mazF* gene was then inserted downstream of HIV-1 U3-TAR resulting in the self-inactivating retroviral vector, pMTD3-U3TAR-MazF. As a control, the GFP gene was inserted in place of the *mazF* gene, which resulted in pMTD3-U3TAR-GFP. The self-inactivating retroviral vectors were generated using the transient transfection method with the packaging plasmids MoMLV-gag-pol, GALV-env,
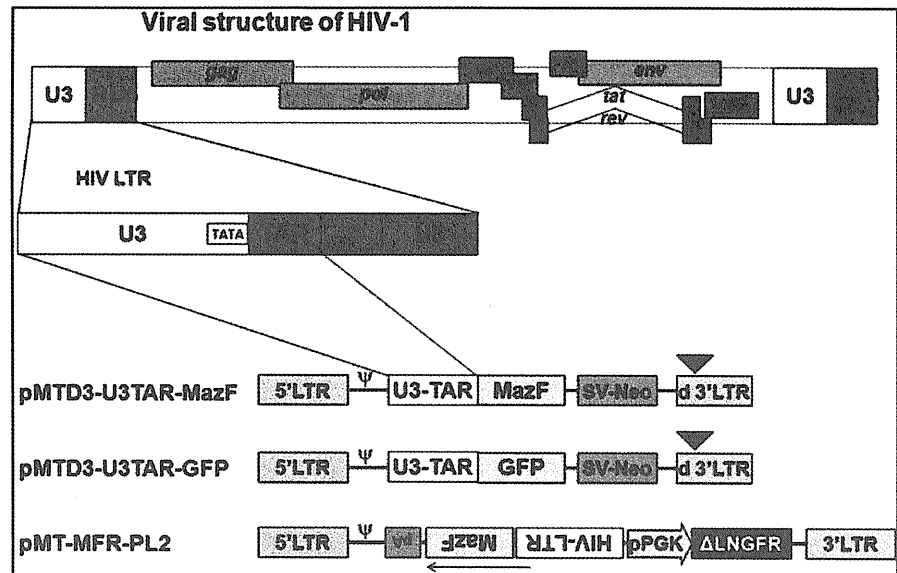
and the self-inactivating retroviral vector in 293T cells. The viral preparation was obtained 2 days after transfection by filtering the culture supernatant. To improve the viral titer for efficient gene transduction over an initial vector, HIV-LTR-MazF-polyA cassette was inserted in the opposite direction of the MoMLV-LTR at the multi-cloning site of pMT. A truncated form of the human low-affinity nerve growth factor gene (ΔLNGFR) (Verzeletti *et al.,* 1998) was used as a surface marker. The resultant vector plasmid was designated pMT-MFR-PL2. GALV-env retroviral vector was generated as described in Materials and Methods.

Retroviral transduction into primary rhesus macaque CD4+ T cells

Rhesus macaque CD4+ T cells were isolated from peripheral blood mononuclear cells (PBMC) using anti-CD4 monoclonal antibody-conjugated beads (Dynal CD4 Positive Isolation Kit; Invitrogen). Prior to gene transduction, the isolated CD4+ T cells were activated for 3 days with a combination of anti-monkey-CD3 clone FN-18 (BioSource, Camarillo, CA) and anti-human-CD28 monoclonal antibody clone L293 (BD Biosciences, Franklin Lakes, NJ)-conjugated beads at a cell-to-bead ratio of 1:1 in GT-T503 (Takara Bio) supplemented with 10% FBS and 200 IU of interleukin-2 (Chiron, Emeryville, CA). On day 3, activated CD4+ T cells were infected with the MazF retroviral vector (MT-MFR-PL2) in the presence of RetroNectin (Takara Bio) as per the manufacturer's instructions. The transduction was repeated again on day 4. The cells were further incubated for another 3 days. The genetically modified cells marked with the ΔLNGFR+ were concentrated with anti-CD271 monoclonal antibody-conjugated beads (CD271 MicroBeads; Miltenyi Biotec, Bergisch Gladbach, Germany). Aliquots of the *mazF* gene-modified cells (designated as MazF-Tmac cells) were collected and cryopreserved until use. As a control, the nontransduced CD4+ T cells were also prepared using the same method as used above.

HIV infection

CEM-SS cells and CEM-SS cells transduced with MTD3-U3TAR-MazF or MTD3-U3TAR-GFP were infected with HIV-1 IIIB at the different multiplicities of infection (MOIs) of 0.07, 0.0007, and 0.00007. After infection, cells were washed with PBS and subsequently cultured in 10 ml of RPMI

1640 containing 10% FBS. HIV-1 p24 levels in the culture supernatant were calculated using the p24 ELISA kit (PerkinElmer, Waltham, MA). Viable cell numbers were measured using the trypan blue exclusion assay. The doubling time of cells was calculated by logistic regression analysis of each growth curve for the HIV-1 infection sets.

SHIV infection

The cryopreserved cells of the control CD4+ T and MazF-Tmac cells were recovered in GT-T503 medium supplemented with 10% FBS and 200 IU of interleukin-2 and reactivated with anti-monkey-CD3 and anti-human-CD28 monoclonal antibody-conjugated beads at a cell-to-bead ratio of 5:1. After a 6-day incubation, the cells were infected with simian/human immunodeficiency virus (SHIV) 89.6P (Reimann *et al.,* 1996) at the MOI of 0.01 and cultured for 6 more days. SHIV RNA levels in the culture supernatant and intracellular RNAs were determined by using quantitative real-time PCR (Thermal Cycler Dice Real Time System; Takara Bio Inc.) with a set of specific primers designed in the SHIV *gag* region (Miyake *et al.,* 2006).

Flow cytometry

Flow cytometry was used for the analysis of surface CD4 expression and transduction efficiency. Endogenous expression levels of CD4 in CEM-SS cells and CEM-SS cells transduced with MTD3-U3TAR-MazF were analyzed using phycoerythrin (PE)-labeled anti-human CD4 antibody (Beckman Coulter, Fullerton, CA). Intracellular p24 levels were analyzed using fluorescein isothiocyanate-labeled anti-p24 antibody (Beckman Coulter) after the cells were fixed and permeabilized for flow cytometric analysis.

Gene transfer efficiencies of the retroviral Tat expression vector into CEM-SS cells and CEM-SS cells transduced with MTD3-U3TAR-MazF were analyzed by detecting the ZsGreen marker fluorescence. Immediately before flow cytometry, propidium iodide (PI) was added at the concentration of 100 ng/ml to stain dead cells. Samples were run through a FACSCantoII flow cytometer (BD Biosciences), and data were analyzed using the FACSDiva software (BD Biosciences).

Genomic DNA analysis

Genomic DNA was extracted by phenol/chloroform extraction from CEM-SS cells and CEM-SS cells transduced with MTD3-U3TAR-MazF cells infected with HIV-1 IIIB at

the MOI of 0.007. Two different regions of the HIV-1 gag gene (246–467 and 905–1046) were amplified by PCR at 14 days after HIV-1 IIIB infection. As a positive control, genomic DNA was amplified from H9 cells chronically infected with HIV-1 IIIB. Human mitochondrial DNA (mtDNA) was amplified as a control for the PCR.

Co-culture with chronically infected cells

The CEM-SS cell line chronically infected with HIV-1 IIIB (CH-1) was mixed with CEM-SS cells or CEM-SS cells transduced with MTD3-U3TAR-MazF. CH-1 cells were mixed at different ratios of 10, 1, or 0.1%. After 6 and 14 days of infection, intracellular p24 levels were analyzed by flow cytometric analyses.
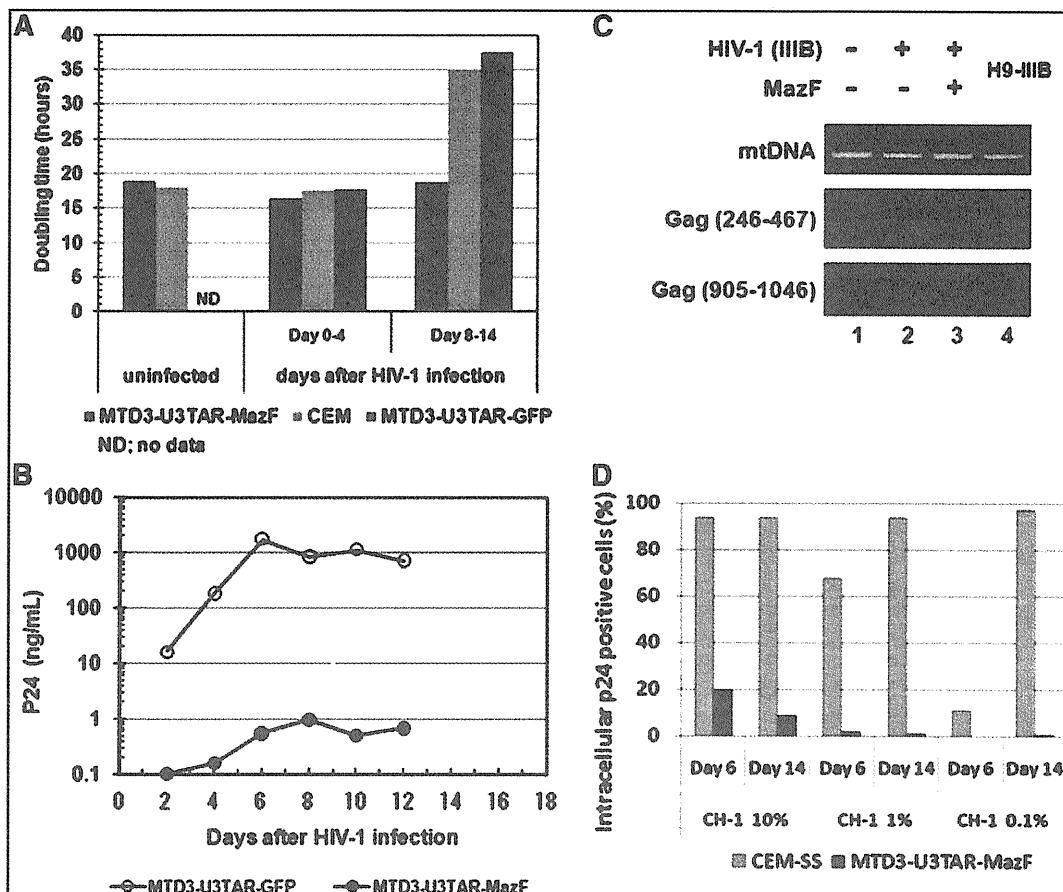

FIG. 2. Analysis of MazF-transduced CEM-SS cells after HIV-1 infection. (A) CEM-SS cells transduced with either the mazF gene or the GFP gene were infected with HIV-1 IIIB at an MOI of 0.07. After infection, the doubling time of the cells for each culture condition was calculated using linear regression analysis using Microsoft Excel software. The square of the correlation coefficient (R^2) between culture day and log (cell number) values was observed to be >0.97. (B) HIV-1 p24 levels in the culture supernatant were estimated using the p24 ELISA kit. Filled circles indicate p24 levels in the supernatant of CEM-SS cells transduced with MTD3-U3TAR-MazF. Open circles indicate p24 levels in the supernatant of CEM-SS cells transduced with MTD3-U3TAR-GFP. (C) Genomic DNA PCR analysis of CEM-SS cells and MazF-transduced CEM-SS cells infected with HIV-1 IIIB at an MOI of 0.007. Two different regions of the HIV-1 gag gene (246–467 and 905–1046) were amplified by PCR at 14 days after HIV-1 IIIB infection. As a positive control, the genomic DNA was amplified from H9 cells chronically infected with HIV-1 IIIB. Human mtDNA was amplified as a control for the PCR reaction. (D) Intracellular p24 levels were analyzed in the mixtures of CEM-SS cell lines chronically infected with HIV-1 IIIB (CH-1) using CEM-SS cells or MazF-transduced CEM-SS cells. CH-1 cells were mixed at different ratios of 10, 1, or 0.1%. After 6 and 14 days of infection, cells were stained with an anti-HIV-1 p24 antibody and subjected to flow cytometric analysis.

Results

We first constructed the retroviral vector system in which the gene for MazF was inserted downstream of the HIV-1 TAR sequence (Fig. 1). As the *E. coli mazF* gene contains nine ACA sequences in its open-reading frame, all of these ACA sequences were first engineered to other MazF-uncleavable sequences without altering the amino acid sequence of MazF to make the *mazF* mRNA resistant to MazF. The resulting self-inactivating retroviral vector (MTD3-U3TAR-MazF) was used to transduce CD4+ T lymphoid CEM-SS cells to create a system in which MazF induction in CEM-SS cells upon infection with HIV-1 effectively suppressed HIV-1 replication without causing apoptosis of infected T cells. The MTD3 retroviral vector contained an intact 5′ LTR and a mutated 3′ LTR that lacks most of the transcriptional elements present in U3. Cells transduced with the resulting retroviral vector contained the defective LTR at both ends (Yu *et al.*, 1986). The self-inactivating retroviral vector was transiently produced and subsequently transduced into the human T lymphoid line CEM-SS cells, which are highly susceptible to HIV infection. Transduced cells were subjected to G418 selection to obtain drug-resistant populations. A GFP-expressing retroviral vector under the control of HIV-LTR (MTD3-U3TAR-GFP) was also used as a control.

The growth rate of CEM-SS cells transduced with MTD3-U3TAR-MazF was comparable to that of the parental CEM-SS line (Fig. 2A), suggesting that MazF expression was tightly controlled and did not inhibit cell growth. Furthermore, the CD4 levels of MTD3-U3TAR-MazF-transduced CEM-SS cells were identical to those of the parental CEM-SS cells (Fig. 3A).

To investigate the effects of HIV-1 infection, MazF-transduced or GFP-transduced CEM-SS cells were infected with HIV-1 IIIB at different MOIs, specifically 0.07, 0.0007, and 0.00007 (Fig. 4). Levels of the HIV-1 p24 antigen in the culture media were examined 16 days post infection. As shown in Fig. 4, in MazF-transduced CEM-SS cells, HIV-1 replication was effectively suppressed. To more precisely investigate the antiviral effects of MazF, viral production and cell growth were measured every other day after HIV-1 IIIB infection at the MOI of 0.07. As shown in Fig. 2A, in the beginning of the culture from day 0 to day 4, cell growth was similar among CEM-SS cells, MazF-transduced CEM-SS cells, and GFP-transduced CEM-SS cells, as well as uninfected CEM-SS cells. CEM-SS cells harboring the *mazF* (ACA-less) gene grew at a normal rate throughout the time course of HIV-1 IIIB infection, whereas both GFP-transduced CEM-SS cells and the parental cell line showed aberrant growth rates due to HIV-1 infection in late cultures after day 8 (Fig. 2A). Indeed, a high level of p24 was detected in the GFP-transduced cell populations during the course of infection (Fig. 2B). In the case of MazF-transduced cells, however, levels of p24 were three orders of magnitude lower than those of GFP-transduced cells throughout the experiment (Fig. 2B). Notably, CD4 levels of MazF-transduced cells infected with HIV-1 IIIB were largely unaffected (Fig. 3B). Together with the fact that the HIV-1 IIIB infected cells harboring the *mazF* gene grew normally (Fig. 2A), these results suggest that HIV-1 IIIB gene expression in the HIV-1-LTR-regulated *mazF* (ACA-less)-transduced cells is effectively inhibited by blocking HIV-1 replication with little damage to cellular function.
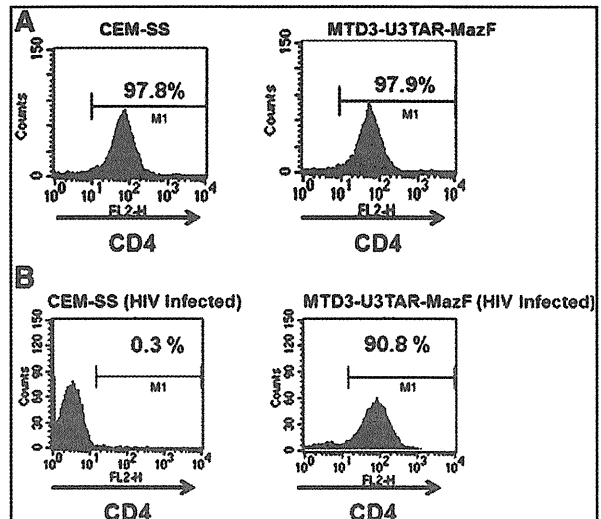

FIG. 3. CD4 levels in MazF-transduced cells. (A) Endogenous expression levels of CD4 were analyzed using PE-labeled anti-human CD4 antibody following flow cytometric analysis. (B) CEM-SS control cells and CEM-SS cells transduced with MTD3-U3TAR-MazF were infected with HIV-1 IIIB at an MOI of 0.007. After infection, the cells were maintained for 5 weeks and CD4 expression levels were analyzed using PE-labeled anti-human CD4 antibody following flow cytometric analysis.

Next, we examined if HIV-1 IIIB was integrated into the genome of MazF-transduced CEM-SS cells upon HIV-1 infection. Two different regions of the HIV-1 *gag* gene were amplified by PCR using genomic DNA 14 days after HIV-1 IIIB infection. As shown in Fig. 2C, both regions of the *gag* gene were detected in the genome of MazF-transduced CEM-SS cells, which were resistant to HIV-1 replication (lane 3). Similarly, HIV-1 DNA was detected in the genomes of CEM-SS cells (lane 2) and H9-IIIB cells (lane 4) (positive control H9 cells chronically infected with HIV-1 IIIB), whereas no bands were detected in noninfected cells (lane 1). We also established a CEM-SS cell line chronically infected with HIV-1 IIIB (CH-1). When this cell line was mixed with CEM-SS cells or MazF-transduced CEM-SS cells at a ratio of 10, 1, or 0.1%, CEM-SS cells were gradually infected with HIV-1 produced from CH-1 cells (Fig. 2D) and their cell growth was suppressed. Alternatively, MazF-transduced CEM-SS cells showed no growth inhibition (data not shown), indicating that HIV-1 replication was suppressed in MazF-transduced CEM-SS cells. As a result, the culture was eventually taken over by normally growing MazF-transduced CEM-SS cells over the slow-growing CH-1 cells. These data demonstrate that MazF-transduced cells are resistant to HIV-1 IIIB infection by blocking HIV-1 IIIB replication.

To investigate the *mazF* gene expression and subsequent effects more precisely, CEM-SS cells and CEM-SS cells transduced with MTD3-U3TAR-MazF were infected with the Tat-expressing retroviral vectors, M-LTR-Tat-ZG or H-LTR-Tat-ZG (Fig. 5A). Induction of the *mazF* gene in CEM-SS cells transduced with MTD3-U3TAR-MazF was monitored by real-time PCR, and the relative ratios were compared with mock infection (Fig. 5B). Infected cells were also subjected to
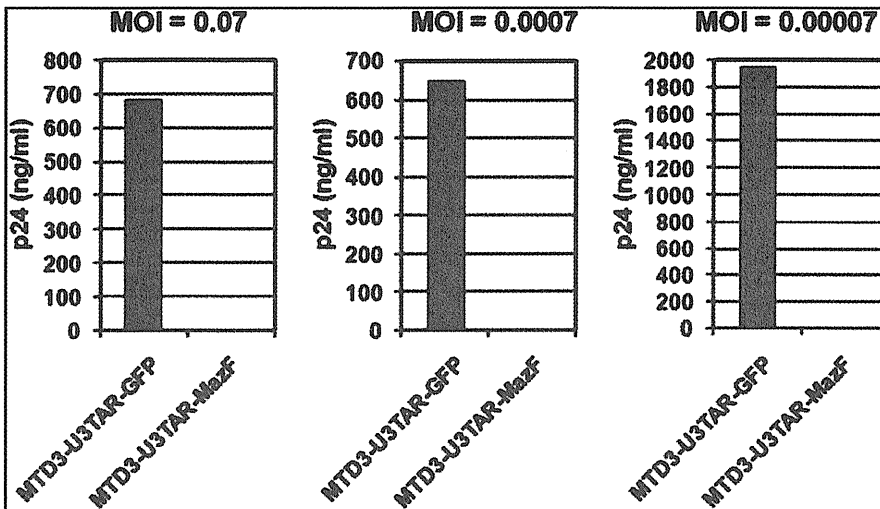
FIG. 4. HIV-1 IIIB infection using MazF-transduced CEM-SS cells at different MOIs. Polyclonal cell populations of CEM-SS resulting from gene transduction with retroviral vectors MTD3-U3TAR-MazF or MTD3-U3TAR-GFP were infected with HIV-1 IIIB at different MOIs (0.07, 0.0007, and 0.00007). Sixteen days after infection, HIV-1 p24 levels in the culture supernatant were estimated using the p24 ELISA kit (PerkinElmer). Given the cytopathic effect of HIV-1, the MTD3-U3TAR-GFP cell population showed delayed proliferation after HIV-1 infection in contrast to the MTD3-U3TAR-MazF population. The delay was more pronounced for the high-MOI group (0.07) than for the low-MOI group (0.00007) at later time points. On day 16 post infection, the accumulated cell number of the high-MOI group was threefold lower than that of the low-MOI group, so the difference in HIV-1 p24 levels between the two MOI groups (0.07 and 0.00007) reflects total cell numbers.

flow cytometry, and both Tat-positive (ZsGreen-positive) cells and dead cells (PI-positive) were monitored (Fig. 5B). As shown in Fig. 5B, strong induction of *mazF* expression was observed upon constitutive M-LTR-Tat-ZG vector transduction, and there was a significant decline in Tat-positive (ZsGreen-positive) cell population. On the other hand, *mazF* induction in HIV-LTR-driven Tat expression was lower, and the influence on cell death was also less than by MLV-LTR-driven Tat expression as observed in the PI-positive population.

lation. Although these experiments do not directly reflect HIV-1 replication, these data support the hypothesis that only low levels of MazF are expressed upon HIV-1 infection and MazF-positive cells can survive with HIV-1 provirus.

As the SIN-based retroviral vector contains the *mazF* gene in the normal orientation, the *mazF* gene is expressed from viral mRNA, resulting in the degradation of the viral RNA and thus significantly reducing the viral titer from this vector. On the other hand, when the MazF expression cassette is
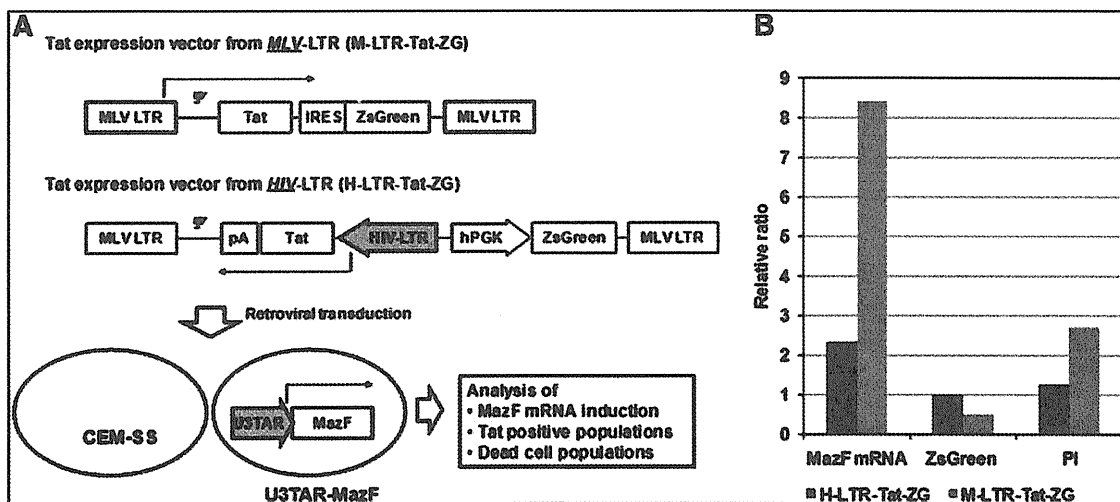

FIG. 5. Analysis of MazF induction upon Tat expression. (A) Outline of experimental procedure to analyze MazF induction upon Tat expression. (B) MazF mRNA levels were analyzed in MTD3-U3TAR-MazF transduced CEM-SS cells after Tat-expressing retroviral vector infection using real-time RT-PCR. The relative fold change is shown compared with that of mock infections. Tat-positive (ZsGreen-positive) cell populations and dead (PI-positive) cell populations in MTD3-U3TAR-MazF-transduced CEM-SS cells were analyzed by flow cytometry 2 days after different Tat retroviral vector transduction. The relative ratio is shown compared with that of CEM-SS cells.

inserted in the opposite direction from the retroviral genome, the viral titer increased and the gene transfer efficiency was improved more than 10 times (data not shown). To investigate the antiviral effect of the TAR-*mazF* system in the primary CD4+ T lymphocytes, the reversely orienting MT-MFR-PL2 vector was introduced into rhesus macaque primary CD4+ T cells from two individual monkeys (#14 and #15). The resulting *mazF*-containing cells were then infected with SIV/HIV-1 chimeric virus SHIV 89.6P. As the SHIV 89.6P harbors HIV-1-derived *env, rev, vpu,* and *tat* genes, the TAR-*mazF* system is expected to function when MazF-Tmac cells are infected with SHIV 89.6P. Indeed, efficient suppression of SHIV 89.6P replication was observed for both primary cell lines, #14 and #15 (Fig. 6A).

To evaluate further how well the retroviral *mazF* system is able to suppress viral RNA production, total cellular RNAs were extracted from MazF-Tmac cells to estimate quantitatively the amounts of SHIV RNA, as well as the mRNAs for ribosomal protein L13a (RPL13a, XM_001093017) and β-actin (NM_001033084), by real-time PCR. The relative ratios were normalized by using 18S rRNA (FJ436026), which is protected from MazF cleavage in ribosomes (Shimazu et al., 2007). We obtained similar results in MazF-Tmac cells from both #14 and #15 primary cell lines. Representative results from MazF-Tmac cells from #14 are shown in Fig. 6B, where one can see that SHIV RNA was preferentially cleaved, whereas the cellular mRNAs were not affected. These results clearly demonstrate that MazF induction from the Tat system upon SHIV 89.6P infection leads to severe defect in maintaining SHIV 89.6P RNA but does not affect cellular mRNAs in SHIV-infected CD4+ T cells.

Discussion

This study demonstrates the distinct feasibility of RNase-based strategies for gene therapy. RNase-based strategies may be preferred over RNA-based strategies for HIV therapy, because RNases cleave HIV-RNA to cause permanent damage to HIV RNA function. Additionally, as RNases

function as an enzymatic catalyst, they are required only at low concentrations in the cells to effectively block HIV proliferation. In the present study, the gene for MazF, an ACA-specific mRNA interferase, was engineered under the HIV-1 LTR promoter and inserted in the genome of the CD4+ T lymphoid cells so that MazF is expected to be produced only when the cells are infected with HIV-1 to produce the Tat protein. We demonstrated that *mazF*-Tmac cells indeed acquired resistance against SHIV replication, but cell growth was not inhibited after SHIV infection (data not shown), indicating that cellular mRNAs were not significantly affected. Notably, MazF was also able to function against the expression of SHIV proviral genome, because the production of SHIV in the culture supernatant was dramatically reduced.

Acquisition of HIV-1 resistance, and more remarkably the ability of MazF-transduced cells to suppress HIV-1 replication, may be explained as follows: Upon HIV-1 infection, Tat expression is first induced from the HIV-1 proviral genome. Tat then triggers the transcription of the *mazF* gene under the LTR promoter, as well as the full-length HIV proviral genome. The resulting induction of MazF expression leads to the cleavage of newly emerged HIV-1 mRNAs so that Tat protein synthesis is no longer sustainable. However, it is important to note that HIV-1 infection does not hamper cell growth and that the HIV-1 provirus genome is retained in the MazF-transduced cells. Therefore, the cellular level of Tat appears to be maintained at a very low level so that the level of MazF induction is also kept very low enough to cleave HIV-1 mRNAs, but not cellular mRNAs. Depending on the integration site and proviral copy number, there might be some MazF-transduced cells that were not resistant to HIV-1 replication. However, these cells could not survive due to HIV-1-induced cell death.

In mammals, virus infection is known to activate the interferon response to induce RNaseL, which mediates degradation of 28S and 18S ribosomal RNAs. This results in inhibition of protein synthesis as part of the host antiviral response (Silverman, 2003). An amphibian ribonuclease,

FIG. 6. Effect of MazF-induction into rhesus macaque primary CD4+ T cells on SHIV 89.6P replication. (A) Rhesus macaque primary CD4 T cells from two monkeys (#14 and #15) were activated and transduced with MT-MFR-PL2 vector. The MazF-transduced cells (MazF-Tmac cells) were reactivated with CD3/28 beads followed by infection with SHIV 89.6P. On days 3 and 6 post infection, culture supernatants were collected and evaluated for SHIV RNA copy by using the quantitative real-time PCR method. (B) Total cellular RNAs extracted from MazF-Tmac cells at 6 days post SHIV 89.6P infection were used to measure the amounts of SHIV RNA, as well as cellular housekeeping mRNAs, by using the quantitative real-time PCR method.
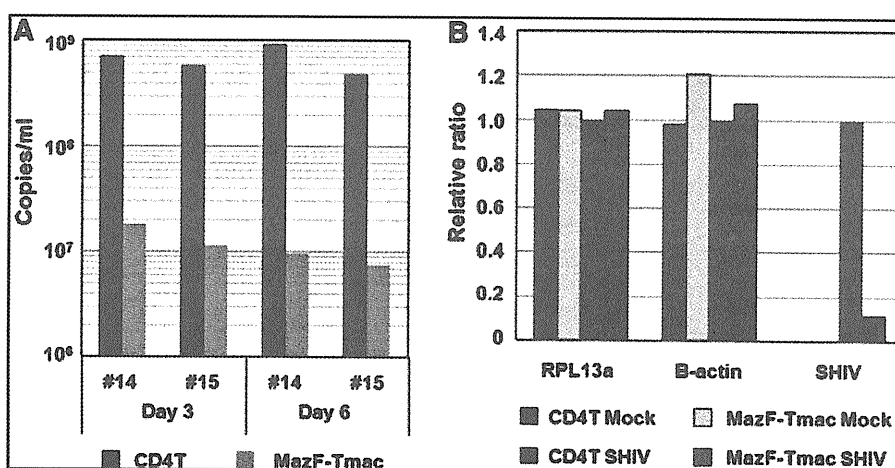
Onconase, is able to inhibit protein synthesis in mammalian cells and has been used as a protein drug. When it was added to the culture media of H9 cells persistently infected with HIV-1, HIV-1 replication was inhibited without blocking cell growth, as degradations of 18S and 28S rRNAs and cellular mRNAs were prevented (Saxena et al., 1996). MazF induction in mammalian cells has shown to cause apoptotic cell death as a result of degradation of cellular mRNAs (Shimazu et al., 2007). However, in the present study, MazF expression induced by HIV-1 Tat appears to be maintained at very low levels, just enough to cleave HIV-1 RNA but not cellular mRNAs, so that cells were able to grow normally. MazF expression may be autoregulated in the cell in such a way that when Tat-induced MazF eliminates invading HIV-1 RNA, Tat expression from the HIV-1 provirus is simultaneously stopped, resulting in simultaneous arrest of MazF production to recover normal cellular functions.

Targeting HIV RNA as a therapeutic strategy using antisense RNA (Levine et al., 2006), ribonucleases (Agarwal et al., 2006), and RNA interference (RNAi) technology (Morris and Rossi, 2004) has been attempted. However, the use of antisense RNA and RNAi technology has not been effective as an anti-HIV technology, as HIV can easily circumvent these RNA inhibitors by creating mutations at the target sequence regions (Lee and Rossi, 2004). On the other hand, the present strategy using MazF targets abundant ACA sequences in HIV-1 RNA (>240), so that it is not possible for HIV-1 to escape from MazF attack by mutations. Furthermore, because MazF has no homology to any mammalian ribonucleases, MazF mRNA interferase activity cannot be inhibited by ribonuclease inhibitors existing in mammalian cells.

In summary, the use of MazF appears to be a novel and highly effective tool for anti-HIV gene therapy. It is effectively able to suppress HIV-1 replication, preventing the emergence of mutated HIV-1. Importantly, MazF induction by invading HIV-1 shows little toxicity to host cells while it efficiently suppresses HIV-1 replication. Specific inhibition of HIV-1 replication by MazF without affecting cell growth is the key feature of MazF-based HIV-1 gene therapy. This may be the first step for RNase-based HIV-1 gene therapy with efficacy *in vitro*. The feasibility of the MazF-based *ex vivo* gene therapy may be verified using autologous CD4+ T lymphocytes from HIV-1 patients. To use our *mazF* vector system for gene therapy, its safety has to be critically evaluated and it should not have any negative impacts on T-cell function. For example, it needs to be shown that there is no alteration in the secretion of functionally important cytokines even though it was observed that MazF expression in HIV-infected CD4+ T cells does not inhibit cell growth. We are currently addressing this question.

Author Disclosure Statement

No competing financial interests exist.

References

Agarwal, S., Nikolai, B., Yamaguchi, T., Lech, P., and Somia N.V. (2006). Construction and use of retroviral vectors encoding the toxic gene barnase. Mol. Ther. 14, 555–563.

Berkhout, B., Silverman, R.H., and Jeang, K.T. (1989). Tat trans-activates the human immunodeficiency virus through a nascent RNA target. Cell 59, 273–282.

Kim, S., Ikeuchi, K., Byrn, R., Groopman, J., and Baltimore, D. (1989). Lack of a negative influence on viral growth by the nef gene of human immunodeficiency virus type 1. Proc. Natl. Acad. Sci. U.S.A. 86, 9544–9548.

Lee, J.T., Yu, S.S., Han, E., Kim, S., and Kim, S. (2004). Engineering the splice acceptor for improved gene expression and viral titer in an MLV-based retroviral vector. Gene Ther. 11, 94–99.

Lee, N.S., and Rossi, J.J. (2004). Control of HIV-1 replication by RNA interference. Virus Res. 102, 53–58.

Levine, B.L., Humeau, L.M., Boyer, J., MacGregor, R.R., Rebello, T., Lu, X., Binder, G.K., Slepushkin, V., Lemiale, F., Mascola, J.R., Bushman, F.D., Dropulic, B., and June, C.H. (2006). Gene transfer in humans using a conditionally replicating lentiviral vector. Proc. Natl. Acad. Sci, U.S.A. 103, 17372–17377.

Miyake, A., Ibuki, K., Enose, Y., Suzuki, H., Horiuchi, R., Motohara, M., Saito, N., Nakasone, T., Honda, M., Watanabe, T., Miura, T., and Hayami, M. (2006). Rapid dissemination of a pathogenic simian/human immunodeficiency virus to systemic organs and active replication in lymphoid tissues following intrarectal infection. J. Gen. Virol. 87, 1311–1320.

Morris, K.V., and Rossi, J.J. (2006). Lentivirus-mediated RNA interference therapy for human immunodeficiency virus type 1 infection. Hum. Gene Ther. 17, 479–486.

Nariya, H., and Inouye, M. (2008). MazF, an mRNA interferase, mediates programmed cell death during multicellular Myxococcus development. Cell 132, 55–66.

Reimann, K.A., Li, J.T., Voss, G., Lekutis, C., Tenner-Racz, K., Racz, P., Lin, W., Montefiori, D.C., Lee-Parritz, D.E., Lu, Y., Collman, R.G., Sodroski, J., and Letvin, N.L. (1996). An env gene derived from a primary human immunodeficiency virus type 1 isolate confers high in vivo replicative capacity to a chimeric simian/human immunodeficiency virus in rhesus monkeys. J. Virol. 70, 3198–3206.

Saxena, S.K., Gravell, M., Wu, Y.N., Mikulski, S.M., Shogen, K., Ardelt, W., and Youle, R.J. (1996). Inhibition of HIV-1 production and selective degradation of viral RNA by an amphibian ribonuclease. J. Biol. Chem. 271, 20783–20788.

Shimazu, T., Degenhardt, K., Nur-E-Kamal, A., Zhang, J., Yoshida, T., Zhang, Y., Mathew, R., White, E., and Inouye, M. (2007). NBK/BIK antagonizes MCL-1 and BCL-XL and activates BAK-mediated apoptosis in response to protein synthesis inhibition. Genes Dev. 21, 929–941.

Silverman, R.H. (2003). Implications for RNase L in prostate cancer biology. Biochemistry 42, 1805–1812.

Verzeletti, S., Bonini, C., Marktel, S., Nobili, N., Ciceri, F., Traversari, C., and Bordignon, C. (1998). Herpes simplex virus thymidine kinase gene transfer for controlled graft-versus-host disease and graft-versus-leukemia: clinical follow-up and improved new vectors. Hum. Gene Ther. 9, 2243–2251.

Yamaguchi, Y., and Inouye, M. (2009). mRNA interferases, sequence-specific endoribonucleases from the toxin-antitoxin systems. Prog. Mol. Biol. Transl. Sci. 85, 467–500.

Yu, S.F., von Rüden, T., Kantoff, P.W., Garber, C., Seiberg, M., Rüther, U., Anderson, W.F., Wagner, E.F., and Gilboa, E.

(1986). Self-inactivating retroviral vectors designed for transfer of whole genes into mammalian cells. Proc. Natl. Acad. Sci. U.S.A. 83, 3194–3198.

Yu, S.S., Han, E., Hong, Y., Lee, J.T., Kim, S., and Kim, S. (2003). Construction of a retroviral vector production system with the minimum possibility of a homologous recombination. Gene Ther. 10, 706–711.

Zhang, Y., Zhang, J., Hoeflich, K.P., Ikura, M., Qing, G., and Inouye, M. (2003). MazF cleaves cellular mRNAs specifically at ACA to block protein synthesis in Escherichia coli. Mol. Cell 12, 913–923.

Zhu, L., Zhang, Y., The, J.S., Zhang, J., Connell, N., Rubin, H., and Inouye, M. (2006). Characterization of mRNA interferases from Mycobacterium tuberculosis. J. Biol. Chem. 281, 18638–18643.

Zhu, L., Inoue, K., Yoshizumi, S., Kobayashi, H., Zhang, Y., Ouyang, M., Kato, F., Sugai, M., and Inouye, M. (2009). Staphylococcus aureus MazF specifically cleaves a pentad sequence, UACAU, which is unusually abundant in the mRNA for pathogenic adhesive factor SraP. J. Bacteriol. 191, 3248–3255.

Address correspondence to:
Dr. Ikunoshin Kato
Center for Cell and Gene Therapy
Takara Bio Inc.
Seta 3-4-1
Otsu, Shiga
520-2193, Japan

E-mail: ikukatiku@zeus.eonet.ne.jp

Dr. Masayori Inouye
Department of Biochemistry
Robert Wood Johnson Medical School
675 Hoes Lane
Piscataway, NJ 08854, USA

E-mail: inouye@umdnj.edu

ScienceDirect

SHORT PAPER

Periventricular Leucomalacia (PVL)-like Lesions in Two Neonatal Cynomolgus Monkeys (Macaca fascicularis)

S. Okabayashi[*,†], K. Uchida[‡], H. Nakayama[‡], C. Ohno[*], K. Hanari[*], I. Goto[*] and Y. Yasutomi[†]

* Corporation for Production and Research of Laboratory Primates, Hachimandai 1-1, Tsukuba-shi, Ibaraki 305-0843, † Tsukuba Primate Research Center, National Institute of Biomedical Innovation, Hachimandai 1-1, Tsukuba-shi, Ibaraki 305-0843 and ‡ Laboratory of Veterinary Pathology, Graduate School of Agricultural and Life Sciences, The University of Tokyo, Yayoi 1-1-1, Bunkyo-ku, Tokyo 113-8657, Japan

Summary

Periventricular leucomalacia (PVL) is a lesion of immature cerebral white matter that occurs in the perinatal period. In man, PVL is the predominant form of brain injury and a cause of cerebral palsy and cognitive deficits in premature infants. PVL affects fetuses and newborns, particularly those who have undergone oxygen deprivation as may occur in premature birth. Many clinical and pathological studies of PVL have been performed in man, but there is no clear definition of PVL in animals. A few spontaneous PVL-like cases in puppies or experimental cases in other animal species have been reported. The present study reports the histopathological and immunohistochemical features of PVL-like lesions in two neonatal cynomolgus monkeys. In both cases, there was cerebral white matter necrosis with marked infiltration of lipid-laden phagocytes and a reduction of neurons in the cerebral cortex. In case 1 there was extensive cavitation of the cerebral white matter. In case 2 there was reactive astrocytosis associated with a decrease in oligodendroglial cells and a decrease in cerebral white matter myelin. To our knowledge, this is the first report of PVL-like leucoencephalomalacia in non-human primates.

© 2010 Elsevier Ltd. All rights reserved.

Cerebral white matter injury in premature human infants is a problem of major clinical importance. These injuries take the form of multiple different lesions including intraventricular haemorrhage, post-haemorrhagic hydrocephalus and periventricular leucomalacia (PVL). PVL is the major form of cerebral white matter injury that affects premature infants and is associated with the subsequent development of cerebral palsy. The characteristic lesion of PVL consists of focal periventricular necrosis, with subsequent cyst formation and more diffuse cerebral white matter injury (Khwaja and Volpe, 2008). Although the pathogenesis of PVL remains to be completely elucidated, it is likely that the necrosis of white matter relates to impaired perfusion resulting from hypoxia—ischaemia (Khwaja and Volpe, 2008). An alternative hypothesis proposes that the lesions result from intrauterine infection with direct toxic effects on fetal oligodendrocytes and astrocytes by cytokines (Damman and Levinton, 1997). Risk factors for PVL include prematurity, asphyxia, respiratory distress, septicaemia, chorioamnionitis, arterial hypotension and hypocarbia (Resch et al., 2004).

There is no clear definition of PVL in animals; however, animal models are necessary for understanding the mechanism of PVL in man. Although a few spontaneous PVL-like cases have been described in puppies (Rentmeister et al., 2004) and several experimental cases (Young et al., 1982; Levison et al., 2001; Brazel et al., 2004) have been reported, no model

reliably replicates all aspects of human PVL. Non-human primates have motor functions and cognitive abilities similar to man and have therefore become increasingly important as experimental models for the study of human central nervous system (CNS) disease. However, PVL-like disease has yet to be described in non-human primates. Here, we report two spontaneously arising cases of PVL-like lesions in neonatal cynomolgus monkeys (*Macaca fascicularis*).

Case 1 was a neonatal female cynomolgus monkey from the Tsukuba Primate Research Center (TPRC) that was delivered by caesarean section at 163 days of gestation as the mother had difficulties in parturition associated with profuse vaginal haemorrhage. The neonate did not breathe for several minutes, but was successfully resuscitated. The body weight of the monkey was 290 g and the animal was artificially nursed. Three days later, paralysis of the limbs was observed and the monkey became progressively debilitated due to insufficient sucking of milk. Despite treatment with subcutaneous infusion of 5% glucose solution and emergency medical care, the monkey died naturally 21 days after birth.

Case 2 was a neonatal male cynomolgus monkey born in the TPRC 16 days prior to the expected date of confinement. The mother rejected the neonate and artificial nursing was conducted. Despite the pre-term birth, the body weight of this monkey was 290 g (the average weight of neonatal cynomolgus monkeys in the TPRC is approximately 300–350 g). The next day, paralysis of the limbs was observed and the monkey could not suck sufficient milk. Because this monkey had abnormal breath sounds 3 days after birth, the veterinarian continued treatment with subcutaneous infusion of 5% glucose solution and antibiotics. However, the monkey died naturally 7 days after birth.

Necropsy examination was performed in each case. Tissues were fixed in 10% neutral buffered formalin, processed routinely and embedded in paraffin wax. Sections (3 μm) were stained with haematoxylin and eosin (HE). For immunohistochemistry (IHC), dewaxed sections were pretreated with H_2O_2 0.5% in methanol and then subjected to antigen retrieval by immersion in citric acid buffer (pH 6.0) and heating in an autoclave for 10 min at 121°C. Sections were then incubated free floating in primary antibody solution overnight at 4°C. Primary antibodies were mouse monoclonal antibodies specific for glial fibrillary acidic protein (GFAP, clone LF2, Dako, Glostrup, Denmark; 1 in 200 dilution), CD68 (clone KP1, Dako; 1 in 100 dilution), vimentin (clone 3B4, Dako; 1 in 200 dilution), neurofilament (NF, clone 2F11, Dako; 1 in 100 dilution) and active-caspase-3 (Cas3; Chemicon, Temecula, California; 1 in 100

dilution). Following brief washes with buffer, the sections were incubated sequentially with polymer immunocomplex (Dako) for 30 min. Immunoreactive elements were 'visualized' by treating the sections with 3, 3'-diaminobenzidine tetroxide (Dojin Kagaku, Kunamoto, Japan) followed by counterstaining with haematoxylin.

For double immunolabelling, sections were dewaxed and then stained with 1% Sudan black B to reduce autofluorescence. Following brief washes, sections were incubated free floating overnight at 4°C in solutions containing mouse monoclonal antibody for myelin basic protein (MBP; Chemicon; 1 in 500 dilution) and rabbit polyclonal antibody specific for oligodendrocytes (olig2; IBL, Takasaki, Gunma, Japan; 1 in 500 dilution). Sections were then incubated with AlexaFluor 488-conjugated goat anti-mouse IgG (Invitrogen, Carlsbad, California; 1 in 1,000 dilution) and AlexaFluor 555-conjugated goat anti-rabbit IgG (Invitrogen; 1 in 1,000 dilution) for 1 h at room temperature. The sections were examined with a Digital Eclipse C1 confocal microscope (Nikon, Kanagawa, Japan). Neonatal monkey brain sections (0-day-old animals) were used as normal controls.

Grossly, the neonatal monkeys were emaciated, dehydrated and had pale mucous membranes. Both limbs and the tail had a decreased range of motion and atrophy of limb muscles was observed in each case. Both tracheas were filled with mucus mixed with milk. The lungs were oedematous and hyperaemic and there were several small white nodules (2–3 mm diameter) in all pulmonary lobes in case 2. In case 1, an excessive quantity of cerebrospinal fluid (CSF) had accumulated in the cranial cavity and the volume of the cerebrum appeared reduced. After formalin fixation, cross sections of the cerebrum in case 1 revealed the presence of marked cavitation of the white matter and atrophy of the cortical region (Fig. 1A), whereas multiple foci of softening of the white matter were found in cross sections of the cerebrum in case 2 (Fig. 1B).

Microscopically, in case 1 areas of cavitation or foci of liquefactive necrosis were widespread with loss of all cellular elements from white matter to deep gray matter, with many lipid-filled phagocytes aggregated within the necrotic foci (Fig. 2A). Residual cerebral cortex showed marked reduction in the number of neural cells. The lateral ventricle was enlarged, with hyperaemia of the choroid plexus, and the ependymal layers showed glial cell infiltration and partial exfoliation. Glial cell infiltration, glial nodules and aggregation of lipid-filled phagocytes with formation of cholesterol clefts were found in the periventricular regions of the lateral ventricle. However, the
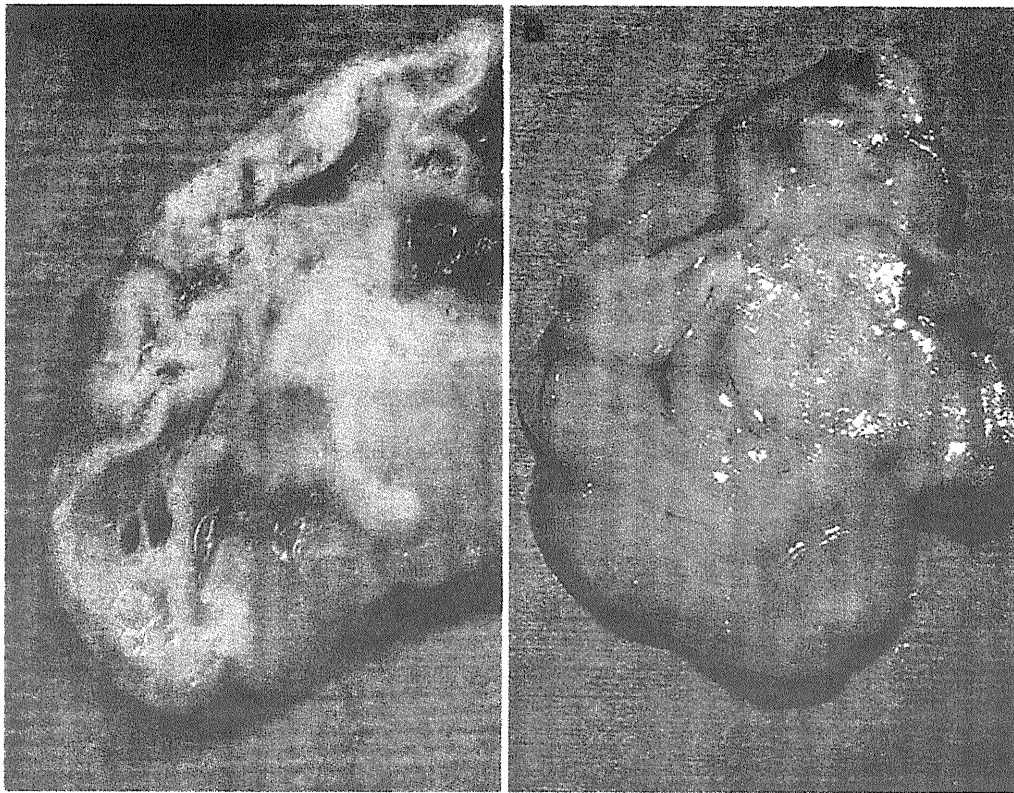
Fig. 1. (A) Cerebrum of a 21-day-old cynomolgus monkey (case 1). Marked cavitation of the white matter and atrophy of the cortical region are present in the temporal lobe. (B) Cerebrum in a 7-day-old cynomolgus monkey (case 2). Multiple foci of white matter softening are present in the temporal lobe.

periventricular regions and ependymal layers of the third ventricle appeared to be largely normal, except for a slight infiltration of glial cells. In case 2, the cerebrum showed massive liquefactive necrosis, with infiltration of lipid-filled phagocytes bilaterally in the temporal white matter and particularly in the periventricular areas of the lateral ventricle. Furthermore, there was diffuse reactive astrocytosis with gemistocytes (Fig. 3A) in various white matter areas and focally in the temporal deep gray matter. The density of neuronal cells was significantly reduced in the lesional sites. Periventricular areas of the third ventricle and thalamus also showed a decrease in neurons infiltration of lipid-filled phagocytes and astrocytosis. Examination of the brainstem, cerebellum, spinal cord and optic nerves did not reveal any abnormalities in either case.

In case 1, immunohistochemical labelling for expression of GFAP revealed apparent proliferation of glial fibrils in the cerebral cortex around cavitations or foci of liquefactive necrosis consistent with glial scar formation (Fig. 2B). In case 2, gemistocytes in the cerebral white matter displayed strong cytoplasmic immunoreactivity for GFAP (Fig. 3A). Immature astrocytes with narrow

cytoplasm and long processes were immunolabelled for GFAP and vimentin (Fig. 3B) in the cerebral cortex and the cerebral white matter. Lipid-filled phagocytes in necrotic foci displayed granular cytoplasmic immunoreactivity for CD68 in both cases (Fig. 2A). Neurons displaying immunoreactivity for NF were significantly reduced in number in each case. Both cases were negative for Cas3 expression, suggesting that the lesions were a result of necrosis rather than apoptosis. Double immunohistochemical labelling with anti-MBP and anti-olig2 was also performed. In normal neonatal monkey brains, some oligodendroglial cells and many myelin sheaths were observed in the white matter (Fig. 4). In contrast, the white matter in case 2 showed a marked decrease in oligodendroglial cells and myelin sheaths (Fig. 4). The white matter in case 1 was unlabelled due to loss of all cellular elements within the areas of cavitation.

In case 1, the lung showed alveolar collapse with proliferation of type II alveolar epithelial cells (AEC II) and infiltration of macrophages into the alveolar space. In case 2, the lung showed severe diffuse pneumonia with infiltration of neutrophils and macrophages into the alveolar space and exfoliation of the alveolar epithelium.
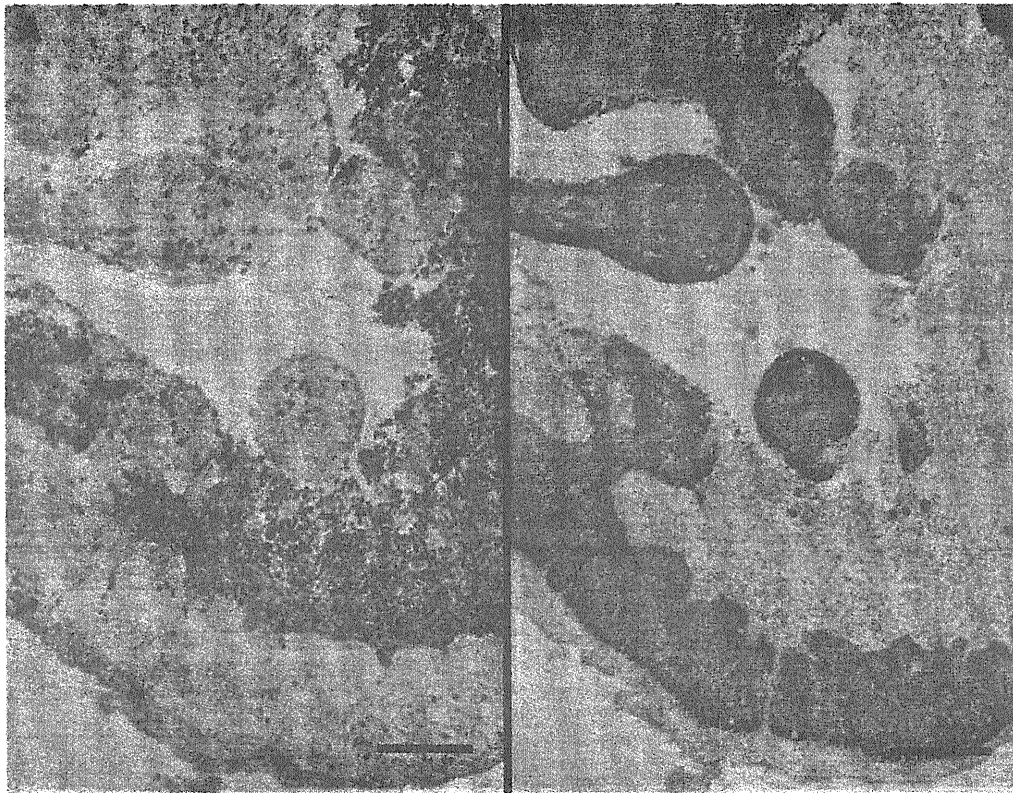
Fig. 2. Cerebrum of a 21-day-old cynomolgus monkey (case 1). (A) There is cavitation or foci of liquefactive necrosis with loss of all cellular elements from white matter to deep gray matter, with aggregation of many lipid-filled phagocytes expressing CD68 in the necrotic foci. IHC. Bar, 200 μm. (B) There is apparent proliferation of glial fibrils around these areas of cavitation or liquefactive necrosis. IHC. Bar, 200 μm.

Some colonies of gram-positive bacteria with morphology consistent with *Staphylococcus* were also observed within the white nodules in the lungs. Additionally, gastric contents, including milk, were found in the trachea of both cases. Atrophy of femoral muscles was observed with proliferation of stromal connective tissue in each case, and this change was particularly severe in case 1. The sciatic nerves of both monkeys appeared almost normal, but there was proliferation of surrounding perineural connective tissue.

Brain injury in the premature human infant consists of multiple lesions, principally germinal intraventricular haemorrhage, post-haemorrhagic hydrocephalus and PVL (Volpe, 2003). PVL refers to injury of the cerebral white matter that occurs with characteristic distribution and consists of focal periventricular necrosis with subsequent cyst formation (cystic PVL) and more diffuse cerebral white matter necrosis with subsequent glial scaring (non-cystic PVL). A third form of cerebral white matter abnormality (the third form of PVL) consists of diffuse astrogliosis without necrosis (Khwaja and Volpe, 2008). PVL is the major form of brain white matter injury that affects premature

human infants and is associated with subsequent development of cerebral palsy, intellectual impairment and visual disturbances. There is currently no specific therapy for PVL (Pierson *et al.*, 2007). The diagnostic hallmarks of PVL are periventricular echodensities or cysts detected by cranial ultrasonography (Deng *et al.*, 2008). Two major factors appear to be involved in the development of PVL. The first involves fetal or neonatal hypoxia—ischaemia that can be a consequence of reduced blood flow to the umbilicus, uterus or placenta in the prenatal or perinatal period. Recent studies suggest that a disturbance of circulation, such as severe hypotension, or cardiogenic shock in preterm infants, such as caused by severe perinatal asphyxia, plays a decisive role in the formation of PVL-lesions (Shankaran *et al.*, 2006; Khwaja and Volpe, 2008). Moreover, experimental studies in which hypoxia is induced artificially have been also conducted in animals for exploration of the pathophysiology of PVL (Painter, 1995; Kohlhauser *et al.*, 2000). Anatomically, early in development, the deep penetrating arteries of the middle cerebral artery that supply the periventricular white matter lack the
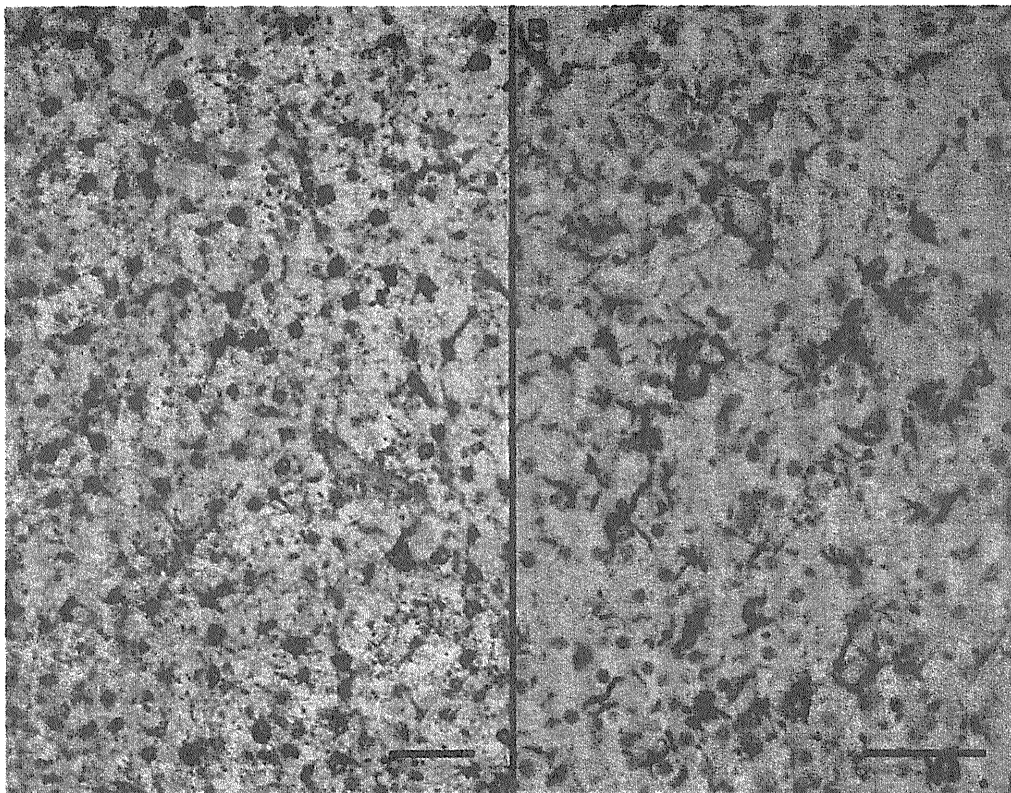
Fig. 3. Cerebrum of a 7-day-old cynomolgus monkey (case 2). (A) Large numbers of reactive astrocytes are present in the cerebral white matter. The cytoplasm of these cells labels for expression of GFAP, an astrocyte-specific marker. IHC. Bar, 50 μm. (B) Premature astrocytes are also present in the cerebral cortex. The narrow cytoplasm and long processes of these cells were immunolabelled for expression of vimentin. IHC. Bar, 50 μm.

vascular anastomoses that help maintain perfusion during periods of hypotension (Takashima *et al.*, 1978; Rorke, 1992; Inage *et al.*, 2000). Therefore, as cerebral autoregulation begins to fail following severe hypotension in neonatal infants, particularly in preterm infants, blood flow is selectively impaired and initially in the white matter of the periventricular region. Furthermore, there is recent evidence that the brain of sick preterm infants often shows impaired cerebrovascular autoregulation in response to change in blood pressure (Soul *et al.*, 2007). This selective hypoperfusion of cerebral white matter during severe hypotension provides a mechanistic explanation for the pathogenesis of PVL. Meanwhile, microglia are activated by the release of reactive oxygen species (ROS) and reactive nitrogen species (RNS), which may mediate cell death. The reactive astrocytes in diffuse lesions could also contribute to the formation of RNS. The release of ROS and RNS by microglia seems likely to result in death of premyelinating oligodendrocytes (pre-OLs) or prevent pre-OLs from differentiating to mature myelin-producing cells in the injured cerebral white matter (Volpe, 2003; Khwaja and Volpe, 2008).

The second major factor contributing to the development of PVL is thought to be maternal intrauterine (or neonatal) infection and fetal (or neonatal) systemic inflammation. Increasing numbers of studies have implicated intrauterine infection in the genesis of PVL. Recent investigations have shown that intravenous injection of the bacterial endotoxin lipopolysaccharide (LPS) can produce selective white matter injury in the neonatal CNS (Paintlia *et al.*, 2008), whereas induction of intrauterine infection can produce diffuse glial cell death and cavitation in fetal white matter (Sherwin and Fern, 2005). The secretion of proinflammatory cytokines such as interleukin (IL)-1, IL-6, and tumor necrosis factor (TNF)-α is known to be toxic to the developing fetal brain (Damman and Levinton, 1997) and may lead to astrogliosis affecting the maturation of myelin-forming oligodendrocytes (Leviton and Gilles, 1996).

The gestation period of the cynomolgus monkey averages 165 days in the TPRC. Case 1 was born on day 163 of gestation and was thus of normal gestational age; however, this animal suffered from a period of asphyxia due to perinatal dystocia. Perinatal asphyxia results from oxygen deprivation that may
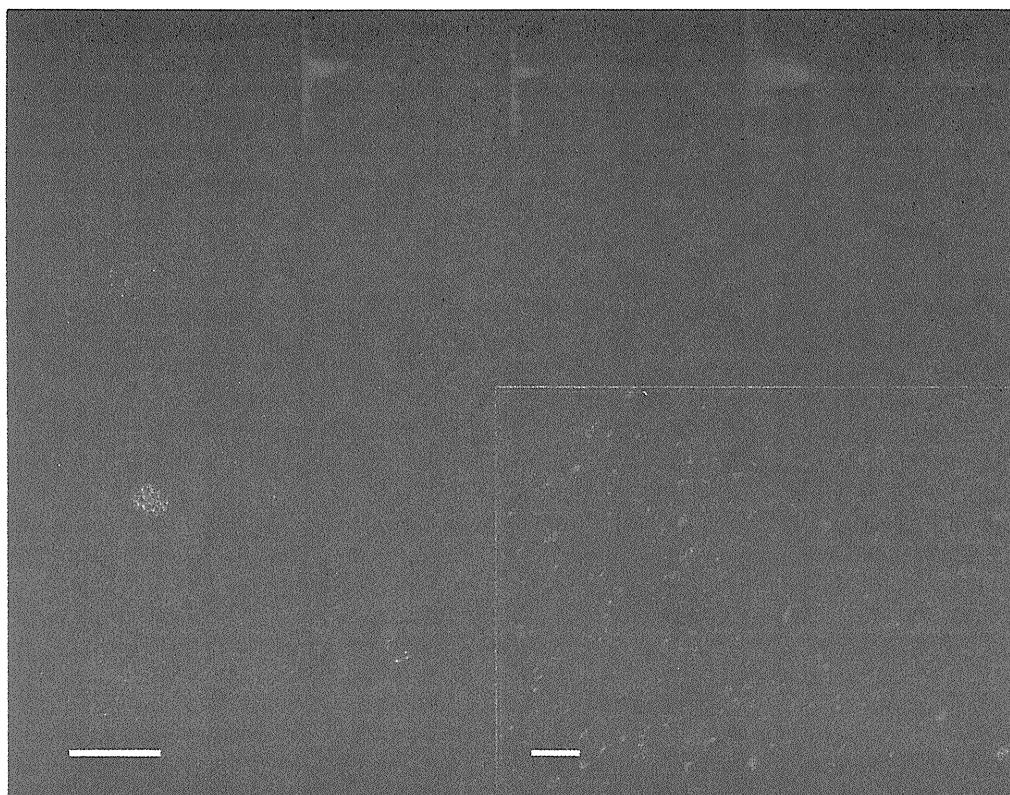
Fig. 4. Cerebrum of a 7-day-old cynomolgus monkey (case 2). Sections were double labelled with antibodies specific for MBP (green) and olig2 (red). There is reduction in cells expressing olig2 and almost no expression of MBP in the cerebral white matter. IHC. Bar, 10 μm. Inset: cerebrum of a normal 0-day-old cynomolgus monkey double labelled as above (control). Within the white matter, oligodendroglial cells express olig2 and many myelin sheaths express MBP. IHC. Bar, 10 μm.

cause harm to the neonatal infant. The condition occurs most commonly due to a drop in maternal blood pressure or interference with blood flow to the brain of the infant during delivery. This was likely to have been the aetiology of the lesions observed in the brain of case 1.

Case 2 was born 16 days before the expected date of confinement. Although PVL may occur in term infants, the injury is more common in premature infants, especially those born between 26 and 34 weeks of gestation (Locatelli et al., 2005). The brain injury in preterm infants is mainly due to the oxidative stress placed on the neonate during delivery (Robles et al., 2001; Haynes et al., 2005), the immaturity of the developing nervous system, and the immaturity of the cerebrovascular supply (Khwaja and Volpe, 2008). Robles et al. (2001) investigated the concentration of hydroperoxides, which are measures of oxidative stress. These authors demonstrated that full-term neonates had levels of hydroperoxides that dropped sharply in the first few hours following birth. However, in premature infants the concentration of hydroperoxides remained at near birth levels for as long as a week and at

dangerously high levels for even longer. Therefore, preterm neonates are at risk of free-radical injury during this period. In addition to these underlying factors, hypoxia—ischaemia can lead to more free-radical production, which can then damage the pre-OLs (Yoshida-Shuto et al., 1992; Robles et al., 2001). Thus, case 2 was at risk of a nervous system disorder and was of especially high risk for developing PVL. A genetic susceptibility to PVL has been proposed with cytokine genes acting as risk modifiers (Baier, 2006), but there was no familial association between the two animals of the present report.

Case 1 had marked cavitation with loss of cellular elements in the cerebral white matter. These changes are similar to cystic PVL and the cavitations may be formed by fusion of multiple cystic foci. Case 2 did not show cavitation, despite the presence of diffuse necrosis of the cerebral white matter, astrogliosis, decreased oligodendroglial cells and marked dysmyelination. These changes are similar to non-cystic PVL or the third form of PVL, and dysmyelination must have been caused by a decrease of myelin-producing oligodendrocytes and disturbance of pre-OL maturation.

The pathological differences between the two monkeys may also have been influenced by the duration of ischaemia or other factors such as fetal age or the length of survival. In general, it is said that microglial reactivity is apparent within 24 h, peaks at 7 days and remains present for weeks following the ischaemia. Phenotypic changes in resident astrocytes occur at 24 h, and these cells proliferate between 48 h and 7 days after ischaemia. Over the ensuing weeks and months, astrocytes increase in number and in fibrillary appearance, eventually resulting in a glial scar or cavitation (Cervós-Navarro and Lafuente, 1991; Williams et al., 2007). Case 1 had widespread cavitation and severe glial scarring, while case 2 showed neuronal decrease, infiltration of lipid-filled phagocytes and astrocytosis in the cerebral white matter and the thalamus. The thalamus is commonly affected in premature infants with PVL (Volpe, 2009), therefore the thalamic lesion in case 2 may have been linked to preterm birth. Furthermore, in each case the femoral muscles showed apparent neurogenic atrophy, likely secondary to dysfunction of the cerebral white matter.

Both monkeys had diffuse pulmonary lesions. In case 1, alveolar collapse was observed with proliferation of AEC II. This may have been caused by artificial ventilation and inhalation of highly concentrated oxygen administered as part of the medical care of the animal. Hyperoxia or hypocarbia results in the death of AEC I and subsequent proliferation of AEC II that differentiate to AEC I to replace the injured or dead AECs during the recovery stages (Takemura and Akamatsu, 1987). Case 2 showed severe purulent alveolar pneumonia with bacterial infection. This bacterial pneumonia may have been due to compromise of the immune system or decreased strength in this premature infant. Both tracheas were filled with a mixture of milk and mucus, suggesting that the animals may have terminally aspirated gastric contents.

Criteria for PVL in animals have not been defined, but the clinical and pathological features of our cases were very similar to those of PVL in man. TPRC has a large-scale breeding colony of experimental cynomolgus monkeys, with about 200 births each year. However, these are the first cases experienced in the TPRC and the first from any primate centre. Future cases should also be subject to ultrasonographic or magnetic resonance imaging investigation. Brain injury in premature infants has an enormous importance to public health because of the large number of such infants who survive with serious neurodevelopmental disability, including major cognitive deficits and motor disability. Because man and monkeys are very similar in anatomy, motor function and cognitive ability, monkeys are favoured as non-human primate models for the

study of post-injury changes in the CNS. These spontaneously arising cases in non-human primates will contribute greatly to understanding the pathophysiology of PVL and to the development of an effective therapy for PVL or cerebral palsy.

References

Baier RJ (2006) Genetics of perinatal brain injury in the preterm infant. Frontiers in Biosciences, 11, 1371—1387.

Brazel CY, Rosti RT, Boyce S, Rothstein RP, Levison SW (2004) Perinatal hypoxia/ischemia damages and depletes progenitors from the mouse subventricular zone. Developmental Neuroscience, 26, 266—274.

Cervós-Navarro J, Lafuente JV (1991) Traumatic brain injuries: structural changes. Journal of Neurological Science, 103, S3—S14.

Damman O, Levinton A (1997) Maternal intrauterine infection, cytokines, and brain damage in the preterm newborn. Pediatric Research, 42, 1—8.

Deng W, Pleasure J, Pleasure D (2008) Progress in periventricular leukomalacia. Archives of Neurology, 65, 1291—1295.

Haynes RL, Baud O, Li J, Kinney HC, Volpe JJ et al. (2005) Oxidative and nitrative injury in periventricular leukomalacia: a review. Brain Pathology, 15, 225—233.

Inage YW, Itoh M, Takashima S (2000) Correlation between cerebrovascular maturity and periventricular leukomalacia. Pediatric Neurology, 22, 204—208.

Khwaja O, Volpe JJ (2008) Pathogenesis of cerebral white matter injury of prematurity. Archives of Disease in Childhood. Fetal and Neonatal Edition, 93, 153—161.

Kohlhauser C, Mosgöller W, Höger H, Lubec B (2000) Myelination deficits in brain of rats following perinatal asphyxia. Life Sciences, 67, 2355—2368.

Levison SW, Rothstein RP, Romanko MJ, Snyder MJ, Meyers RL et al. (2001) Hypoxia/ischemia depletes the rat perinatal subventricular zone of oligodendrocyte progenitors and neural stem cells. Developmental Neuroscience, 23, 234—247.

Leviton A, Gilles F (1996) Ventriculomegaly, delayed myelination, white matter hypoplasia, and 'periventricular' leukomalacia: how are they related? Pediatric Neurology, 15, 127—136.

Locatelli A, Ghidini A, Paterlini G, Patanè L, Doria V et al. (2005) Gestational age at preterm premature rupture of membranes: a risk factor for neonatal white matter damage. American Journal of Obstetrics and Gynecology, 193, 947—951.

Painter MJ (1995) Animal models of perinatal asphyxia: contributions, contradictions, clinical relevance. Seminars in Pediatric Neurology, 2, 37—56.

Paintlia MK, Paintlia AS, Contreras MA, Singh I, Singh AK (2008) Lipopolysaccharide-induced

peroxisomal dysfunction exacerbates cerebral white matter injury: attenuation by N-acetyl cysteine. *Experimental Neurology*, **210**, 560—576.

Pierson CR, Folkerth RD, Billiards SS, Trachtenberg FL, Drinkwater ME *et al.* (2007) Gray matter injury associated with periventricular leukomalacia in the premature infant. *Acta Neuropathology*, **114**, 619—631.

Rentmeister K, Schmidbauer S, Hewicker-Trautwein M, Tipold A (2004) Periventricular and subcortical leukoencephalopathy in two dachshund puppies. *Journal of Veterinary Medicine Series A: Physiology, Pathology and Clinical Medicine*, **51**, 327—331.

Resch B, Jammernegg A, Vollaard E, Maurer U, Mueller WD *et al.* (2004) Preterm twin gestation and cystic periventricular leucomalacia. *Archives of Disease in Childhood. Fetal and Neonatal Edition*, **89**, F315—320.

Robles R, Palomino N, Robles A (2001) Oxidative stress in the neonate. *Early Human Development*, **65**, S75—S81.

Rorke LB (1992) Anatomical features of the developing brain implicated in pathogenesis of hypoxic-ischemic injury. *Brain Pathology*, **2**, 211—221.

Shankaran S, Langer JC, Kazzi SN, Laptook AR, Walsh M (2006) Cumulative index of exposure to hypocarbia and hyperoxia as risk factors for periventricular leukomalacia in low birth weight infants. *Pediatrics*, **118**, 1654—1659.

Sherwin C, Fern R (2005) Acute lipopolysaccharide-mediated injury in neonatal white matter glia: role of TNF-alpha, IL-1beta, and calcium. *Journal of Immunology*, **175**, 155—161.

Soul JS, Hammer PE, Tsuji M, Saul JP, Bassan H *et al.* (2007) Fluctuating pressure-passivity is common in the cerebral circulation of sick premature infants. *Pediatric Research*, **61**, 467—473.

Takashima S, Armstrong DL, Becker LE (1978) Subcortical leukomalacia. Relationship to development of the cerebral sulcus and its vascular supply. *Archives of Neurology*, **35**, 470—472.

Takemura T, Akamatsu H (1987) Ultrastructural study on the pulmonary parenchyma of the neonates following prolonged mechanical ventilation. *Acta Pathologica Japonica*, **37**, 1115—1126.

Volpe JJ (2003) Cerebral white matter injury of the premature infant — more common than you think. *Pediatrics*, **112**, 176—180.

Volpe JJ (2009) Brain injury in premature infants: a complex amalgam of destructive and developmental disturbances. *Lancet Neurology*, **8**, 110—124.

Williams AJ, Wei HH, Dave JR, Tortella FC (2007) Acute and delayed neuroinflammatory response following experimental penetrating ballistic brain injury in the rat. *Journal of Neuroinflammation*, **2**, 4—17.

Yoshida-Shuto H, Yasuhara A, Kobayashi Y (1992) Cerebral blood flow velocity and failure of autoregulation in neonates: their relation to outcome of birth asphyxia. *Neuropediatrics*, **23**, 241—244.

Young RS, Hernandez MJ, Yagel SK (1982) Selective reduction of blood flow to white matter during hypotension in newborn dogs: a possible mechanism of periventricular leukomalacia. *Annals of Neurology*, **12**, 445—448.

BRIEF REPORT

CD16$^+$ natural killer cells play a limited role against primary dengue virus infection in tamarins

Tomoyuki Yoshida · Tsutomu Omatsu · Akatsuki Saito · Yuko Katakai · Yuki Iwasaki · Sayuki Iijima · Terue Kurosawa · Masataka Hamano · Shinichiro Nakamura · Tomohiko Takasaki · Yasuhiro Yasutomi · Ichiro Kurane · Hirofumi Akari

Abstract CD16 is a major molecule expressed on NK cells. To directly assess the role of natural killer (NK) cells in dengue virus (DENV) infection *in vivo*, CD16 antibody-treated tamarins were inoculated with a DENV-2 strain. This resulted in the transient depletion of CD16$^+$ NK cells, whereas no significant effects on the overall levels or kinetics of plasma viral loads and antiviral antibodies were observed in the treated monkeys when compared to control monkeys. It remains elusive whether the CD16$^-$ NK sub-population could play an important role in the control of primary DENV infection.

Keywords Dengue virus · Tamarin · NK cells · CD16

T. Yoshida · Y. Iwasaki · S. Iijima · T. Kurosawa ·
M. Hamano · Y. Yasutomi · H. Akari
Tsukuba Primate Research Center, National Institute
of Biomedical Innovation, 1-1 Hachimandai, Tsukuba,
Ibaraki 305-0843, Japan

T. Yoshida (✉) · A. Saito · H. Akari (✉)
Center for Human Evolution Modeling Research,
Primate Research Institute, Kyoto University, Inuyama,
Aichi 484-8506, Japan
e-mail: ytomoyuki@pri.kyoto-u.ac.jp

H. Akari
e-mail: akari@pri.kyoto-u.ac.jp

T. Omatsu · T. Takasaki · I. Kurane
Department of Virology I, National Institute of Infectious
diseases, 1-23-1 Toyama, Shinjuku-ku, Tokyo 162-8640, Japan

A. Saito
International Research Center for Infectious Diseases,
The Institute of Medical Science, The University of Tokyo,
4-6-1 Shirokanedai, Minato-ku, Tokyo 108-8639, Japan

Y. Katakai
Corporation for Production and Research of Laboratory
Primates, 1-1 Hachimandai, Tsukuba, Ibaraki 305-0843, Japan

S. Nakamura
Research Center for Animal Life Science, Shiga University
of Medical Science, Seta Tsukinowa-cho, Otsu, Shiga 520-2192,
Japan

DENV is one of the most serious mosquito-borne virus affecting humans, with 2.5 billion people at risk in tropical and subtropical regions around the world each year [12]. A wide variety of clinical manifestations have been noted, which range from asymptomatic, mild febrile illness (dengue fever [DF]) to dengue hemorrhagic fever (DHF)/ dengue shock syndrome (DSS), a life-threatening illness. It has been shown that humans with a secondary heterologous DENV infection are at a higher risk of contracting severe dengue disease [10, 26]. DHF/DSS occurs in infants during primary DENV infection, predominantly in the second half of the first year of life, when maternal antibodies have low residual neutralizing activity [11, 17].

NK cells are a component of the innate immune system that plays a central role in host defense against viral infection and tumor cells. It has been shown that infection by some viruses, such as herpes simplex virus-1, influenza virus or ectromelia poxvirus, can be controlled by NK cells in mice [15]. Yet the most compelling evidence for a role

🖄 Springer

of NK cells in early defense against viruses was obtained in a study showing increased susceptibility to murine cytomegalovirus (MCMV) after NK cell depletion and increased resistance after adoptive transfer of NK cells [23]. Defects in NK cell activity, such as decreased production of interferon (IFN)-γ or cytotoxicity, render mice more susceptible to MCMV infection [23]. NK cells can kill virus-infected cells by using cytotoxic granules or by recognizing and inducing lysis of antibody-coated target cells (antibody-dependent cell cytotoxicity) via an Fc-binding receptor such as CD16 [21].

Early activity of NK cells may be important for clearing primary DENV infection [24]. In a DENV mouse model, mice experimentally infected with DENV showed increased NK cell levels [24]. A significant increase in the frequency of NK cell circulation was also shown in patients who developed an acute dengue disease [2]. In addition, patients with a mild dengue disease have elevated NK cell rates when compared to those with severe dengue diseases [9, 27]. Moreover, Kurane et al. [14] reported that human blood NK cells are cytotoxic against DENV-infected cells in target organs via direct cytolysis and antibody-dependent cell-mediated cytotoxicity. It was also shown that the intracellular cytotoxic granule, TIA-1, was up-regulated early in NK cells in the acute phase of DENV infection and that NK-activating receptor NKp44 was involved in virus-mediated NK activation through direct interaction with DENV envelope protein [2, 13]. These results suggest that the early activation of NK cells contributes to the prevention of the severe dengue disease. However, based on quantitative and functional analyses in animal models in vivo, defining the contribution of NK cells to suppression of DENV replication in vivo has been necessary.

We have recently reported that common marmosets (Callithrix jacchus) are highly permissive to DENV infection [22]. These New World monkeys, being nonhuman primates, are considered to have an immune system similar to that of humans [28, 29]. The present study was initiated to investigate the role of NK cells in controlling DENV during primary infection in our nonhuman primate model.

The animals were cared for in accordance with National Institute of Biomedical Innovation rules and guidelines for experimental animal welfare, and all protocols were approved by our Institutional Animal Study Committee. Eight tamarins (Saguinus midas and Saguinus labiatus) were used in this study. As marmosets and tamarins are closely related monkey species and are classified as members of the Callitrichinae, we expected that tamarins would also be permissive to DENV infection, like marmosets. To check the permissiveness of tamarins to DENV, 2 tamarins were infected with DENV-2 (DHF0663 strain: 6.7×10^7 PFU/ml) subcutaneously or intravenously (Fig. 1).
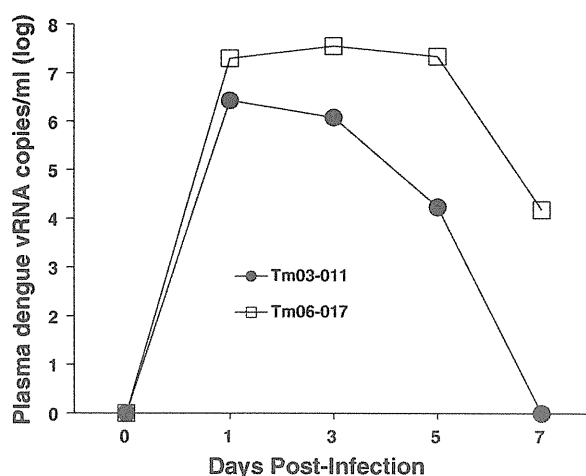

Fig. 1 Levels of vRNA in DENV-infected tamarins. Tamarins were infected subcutaneously or intravenously with DENV at a dose of 6.7×10^7 PFU/ml. The vRNAs were detected in plasma by real-time PCR. Tm03-011, subcutaneous infection; Tm06-017, intravenous infection

Dengue viral RNA (vRNA), which was quantified using real-time PCR as previously described [22], was detected in plasma samples from the tamarins on day 1 post-infection. For each of the two tamarins (Tm03-011, Tm06-017), the plasma vRNA levels reached 2.7×10^6 copies/ml and 2.0×10^7 copies/ml on day 1 post-infection, respectively, and were detectable on days 3 and 5. These results indicate that tamarins are also permissive to DENV infection, which is consistent with the results obtained by using marmosets [22].

Next, we sought to assess the role of NK cells in DENV infection in vivo. In this regard, in vivo depletion of NK cells by the administration of NK-specific monoclonal antibody (mAb) was considered to be straightforward to directly address the question. We employed a new method by which an anti-CD16 mAb 3G8 [7] but not a control mAb MOPC-21 efficiently depleted a major NK population expressing CD16 in tamarins, as we recently reported [29]. The mouse anti-human CD16 mAb 3G8 was produced in serum-free medium and purified using protein A affinity chromatography. Endotoxin levels were confirmed to be lower than 1 EU/mg. Four red-handed tamarins and two white-lipped tamarins (Saguinus labiatus) were used in this experiment. Three tamarins were intravenously administered 3G8 at a dose of 50 mg/kg, while others were given a control mAb MOPC-21. One day later, both mAb-treated tamarins were subcutaneously inoculated with 3×10^5 PFU/ml of DENV-2 DHF0663 strain on the basis of a previous report that a single mosquito might inject between 10^4 and 10^5 PFU of DENV into a human [20]. It was confirmed that at 1-3 days after the 3G8 mAb treatment, CD16$^+$ cells were almost completely depleted in the